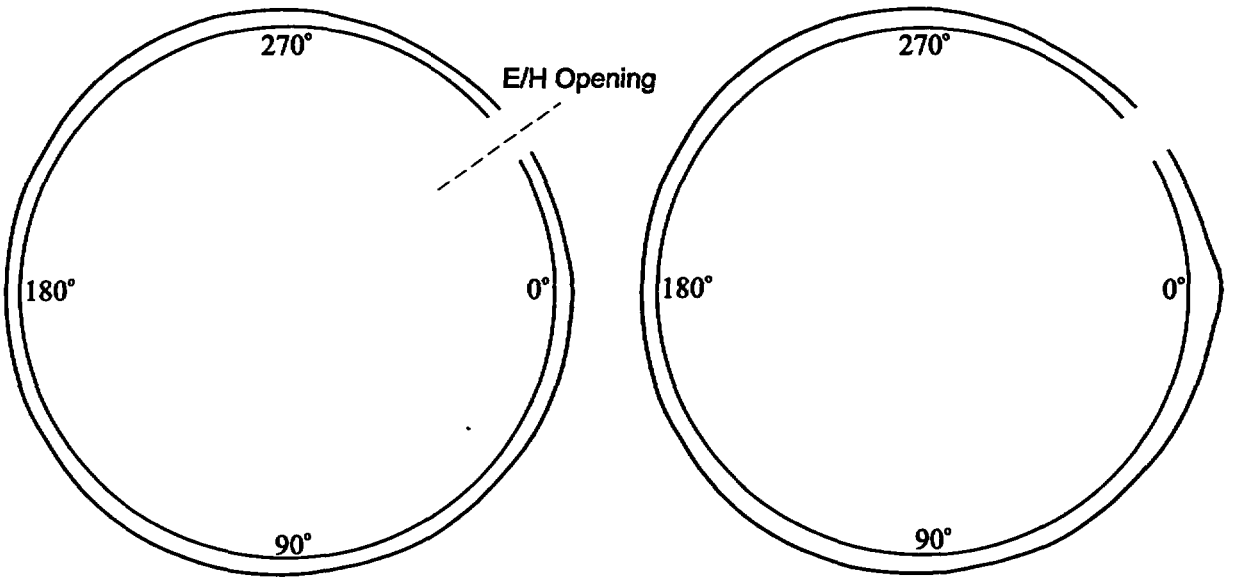

Pressure 1.366 MPa (3.47 Pd)

Pressure 1.373 MPa (3.49 Pd)

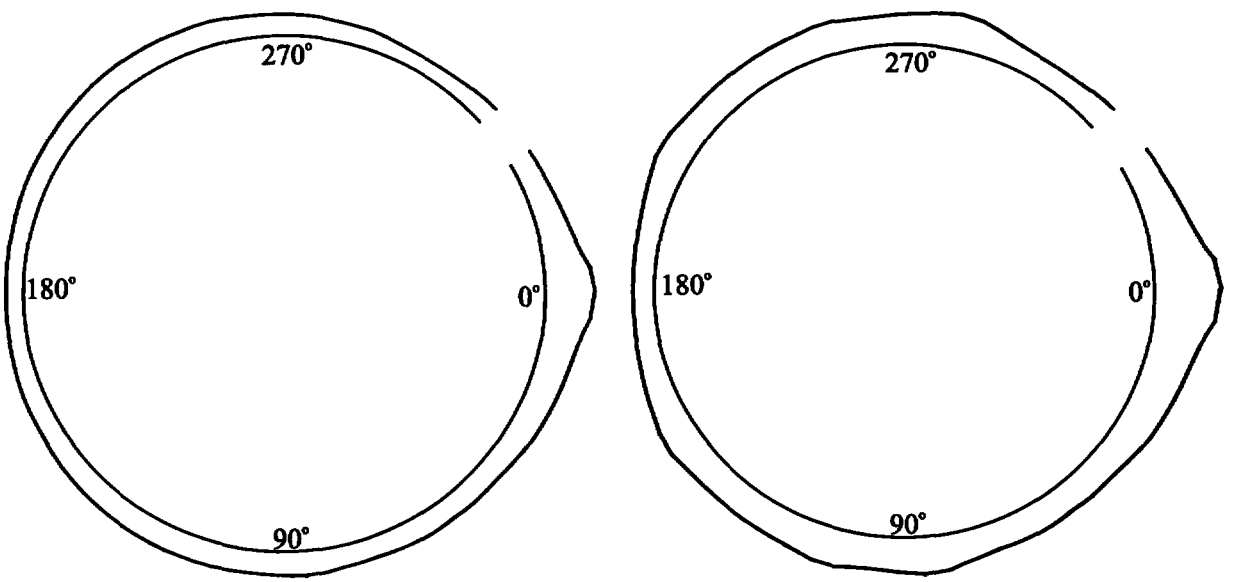

Pressure 1.381 MPa (3.51 Pd)

Pressure 1.389 MPa (3.53 Pd)

Figure 9-26. PCCV SFMT, 3D Global Shell Tendon Rupture Model.
Deformed Shape. For Elevation of 5.4 m. Displacements × 10.

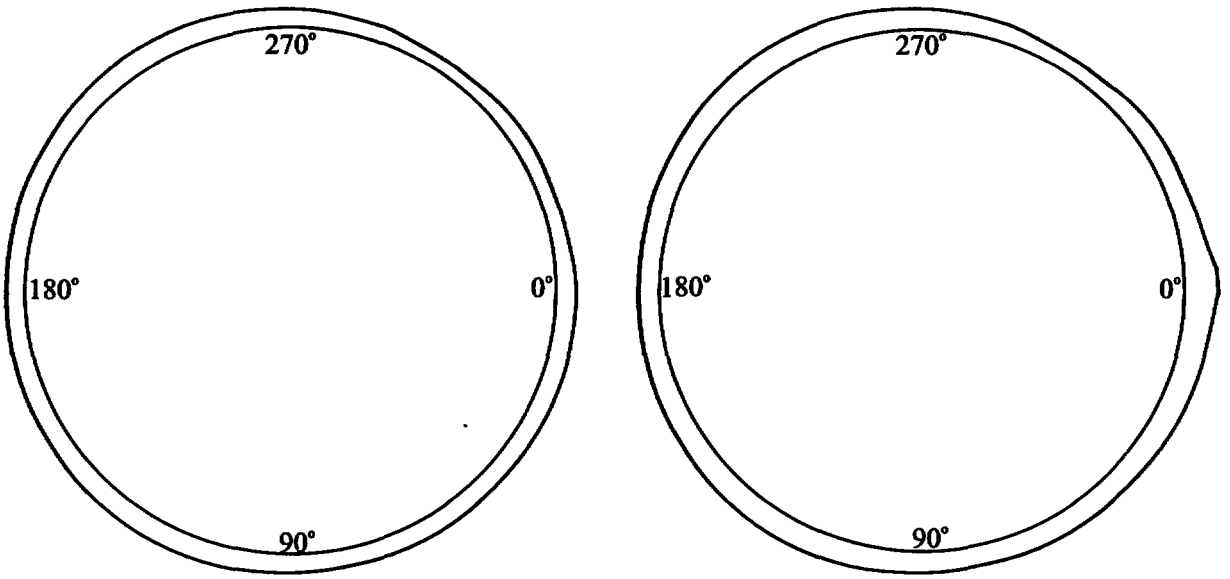

Pressure 1.366 MPa (3.47 Pd)

Pressure 1.373 MPa (3.49 Pd)

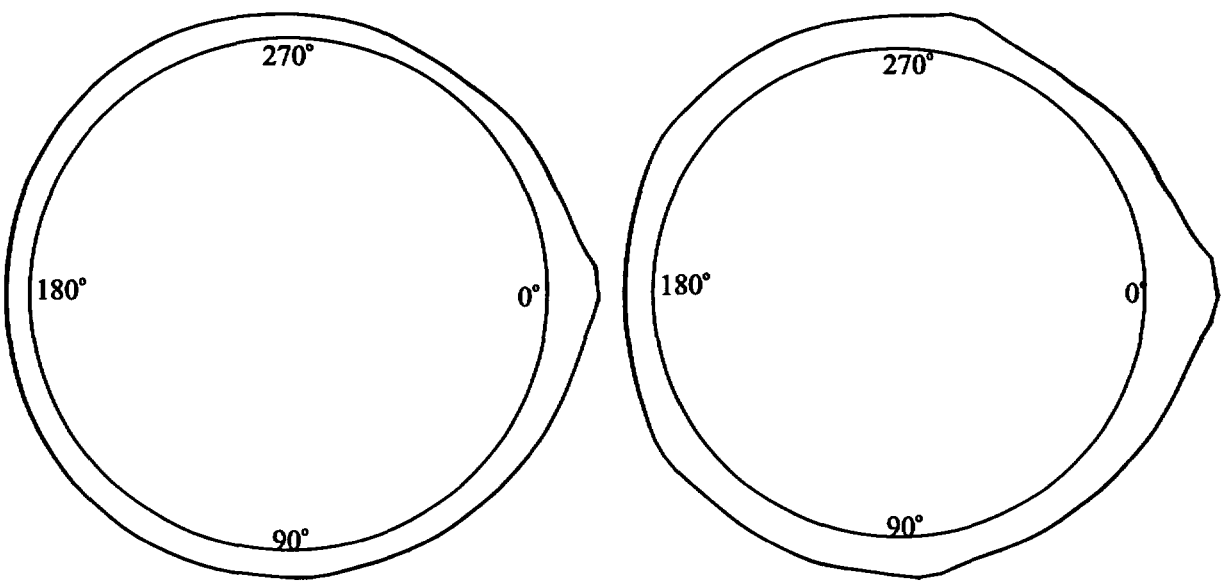

Pressure 1.381 MPa (3.51 Pd)

Pressure 1.389 MPa (3.53 Pd)

Figure 9-27. PCCV SFMT, 3D Global Shell Tendon Rupture Model.
Deformed Shape. For Elevation of 6.5 m. Displacements × 10.

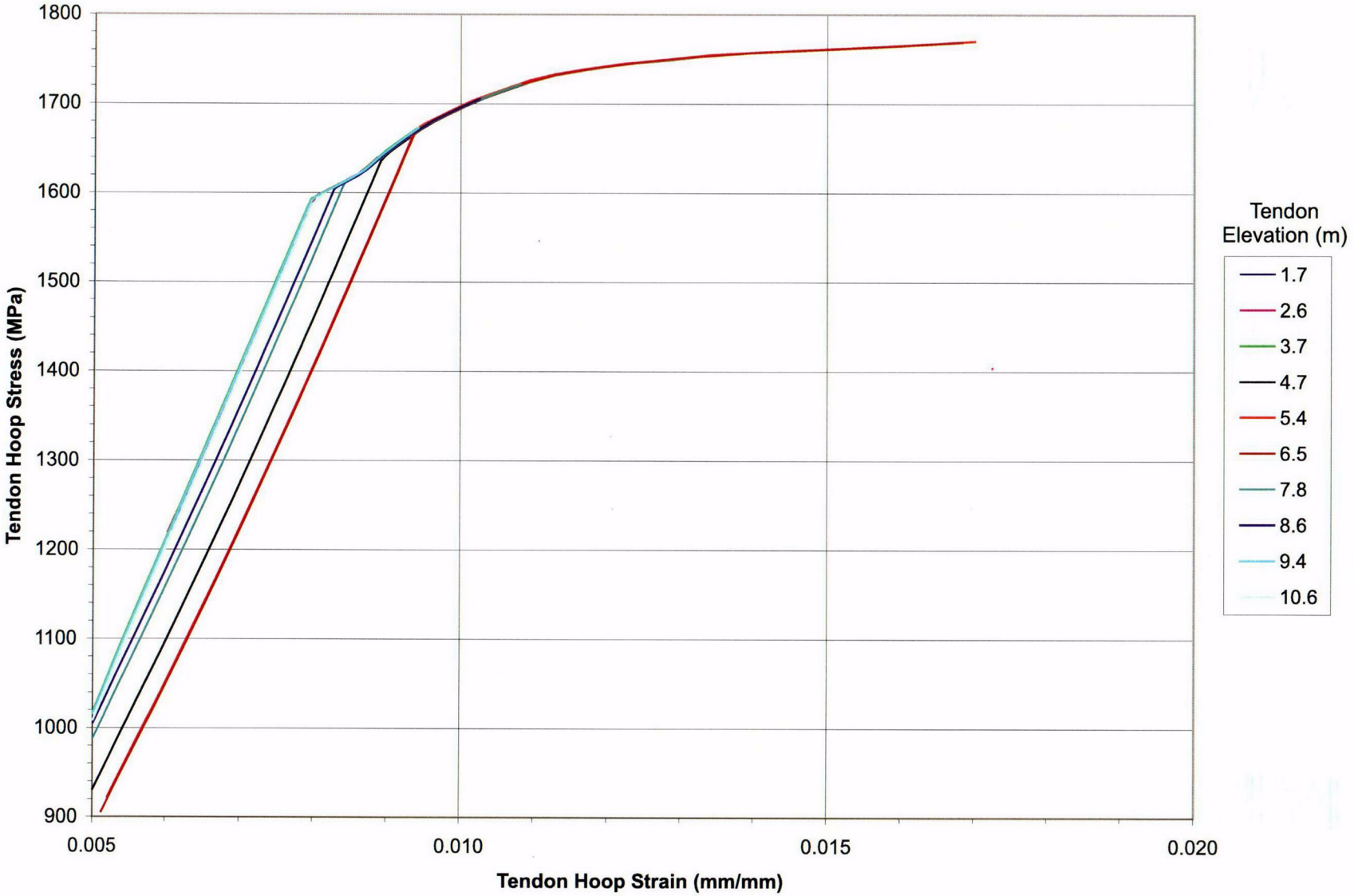

Figure 9-28. PCCV SFMT, 3D Global Shell Model-Hoop Tendon Stress Versus Strain History, Tendon History at 0 Degrees Azimuth, P = 1.357 MPa, 3.45 Pd

C272

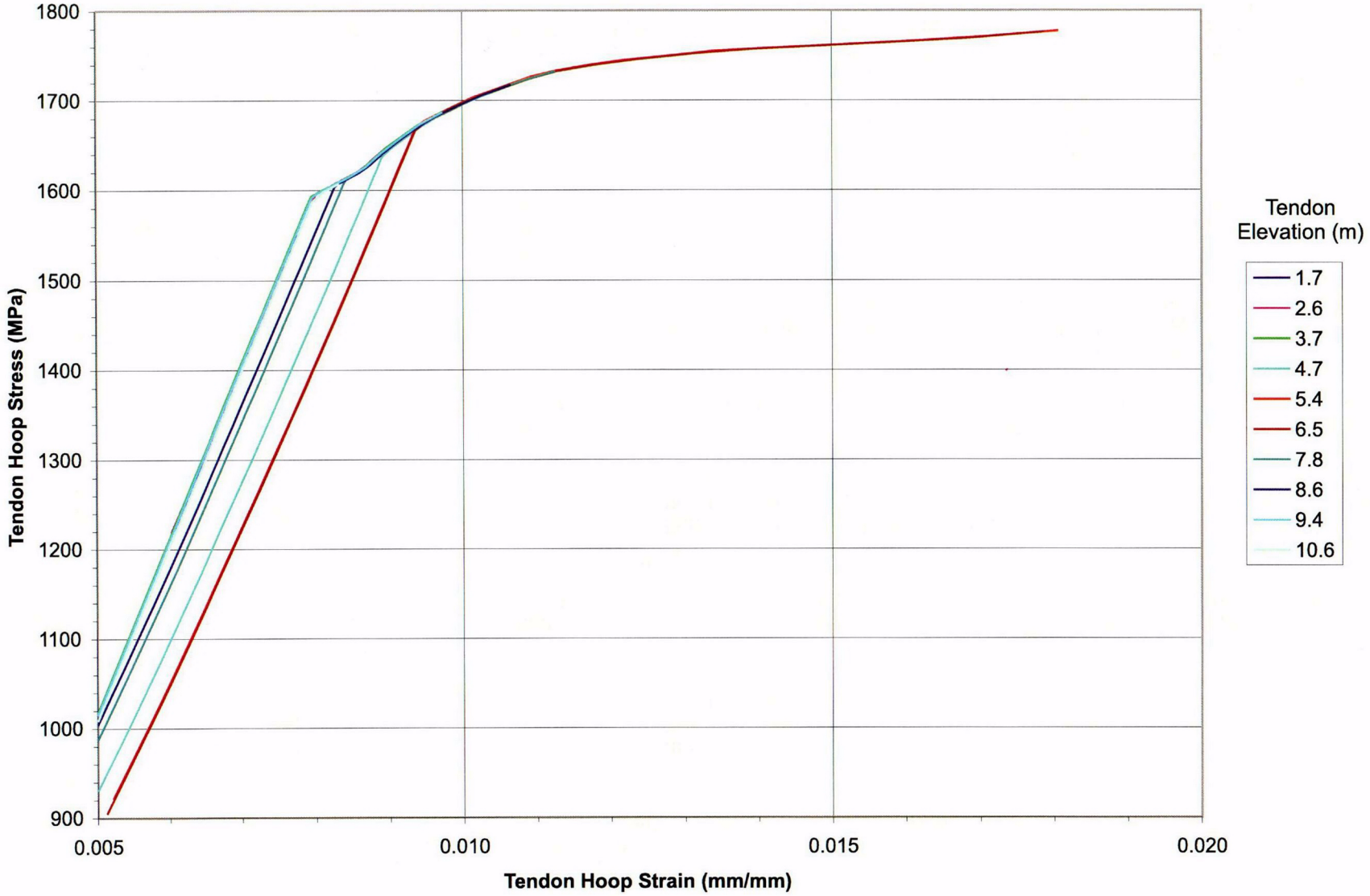

Figure 9-29. PCCV SFMT, 3D Global Shell Model-Hoop Tendon Stress Versus Strain History, Tendon History at 0 Degrees Azimuth, P = 1.366 MPa, 3.47Pd

C273

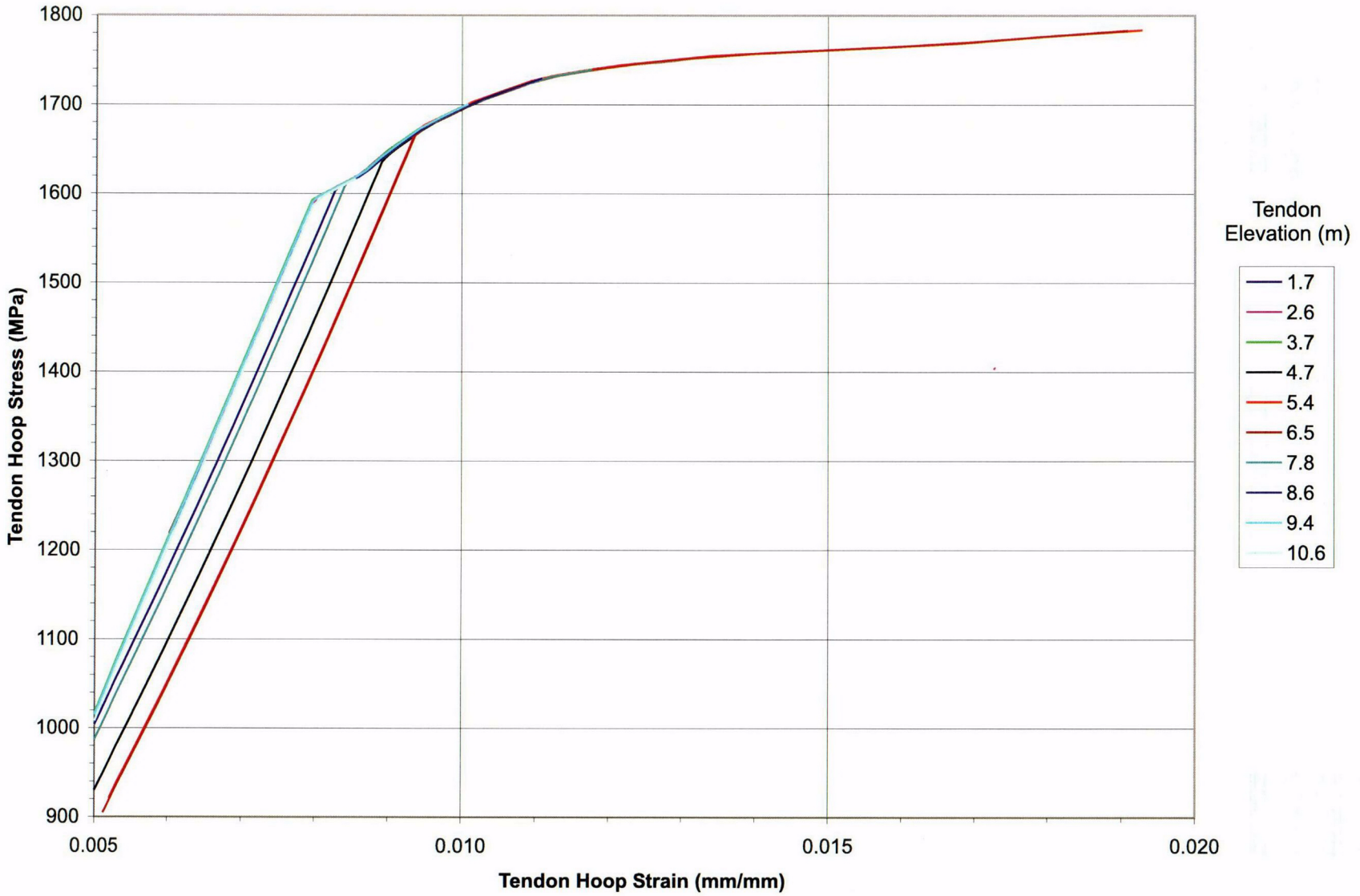

Figure 9-30. PCCV SFMT, 3D Global Shell Model-Hoop Tendon Stress Versus Strain History, Tendon History at 0 Degrees Azimuth, P = 1.373 MPa, 3.49 Pd

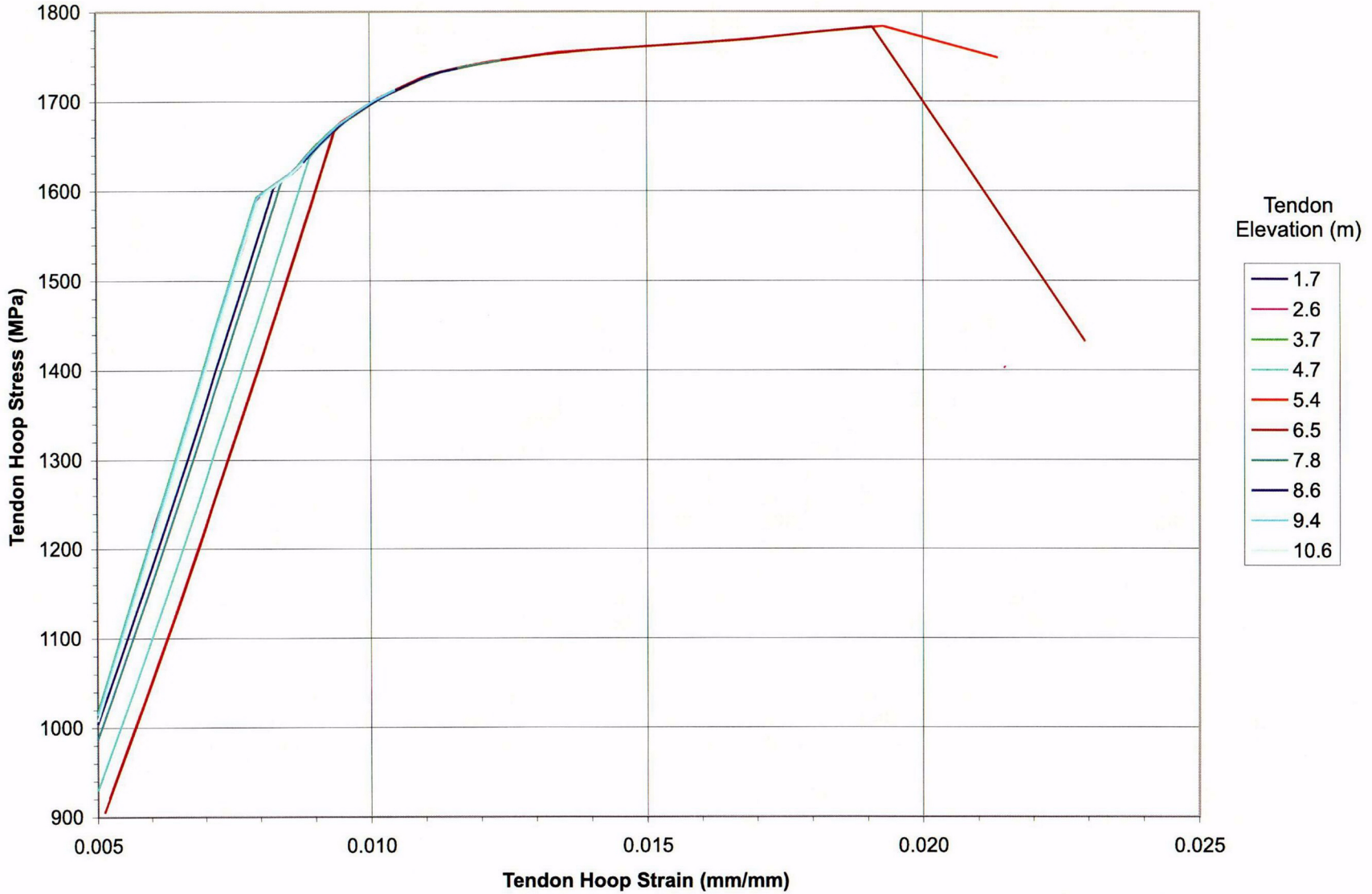

Figure 9-31. PCCV SFMT, 3D Global Shell Model-Hoop Tendon Stress Versus Strain History, Tendon History at 0 Degrees Azimuth, P = 1.381 MPa, 3.51 Pd

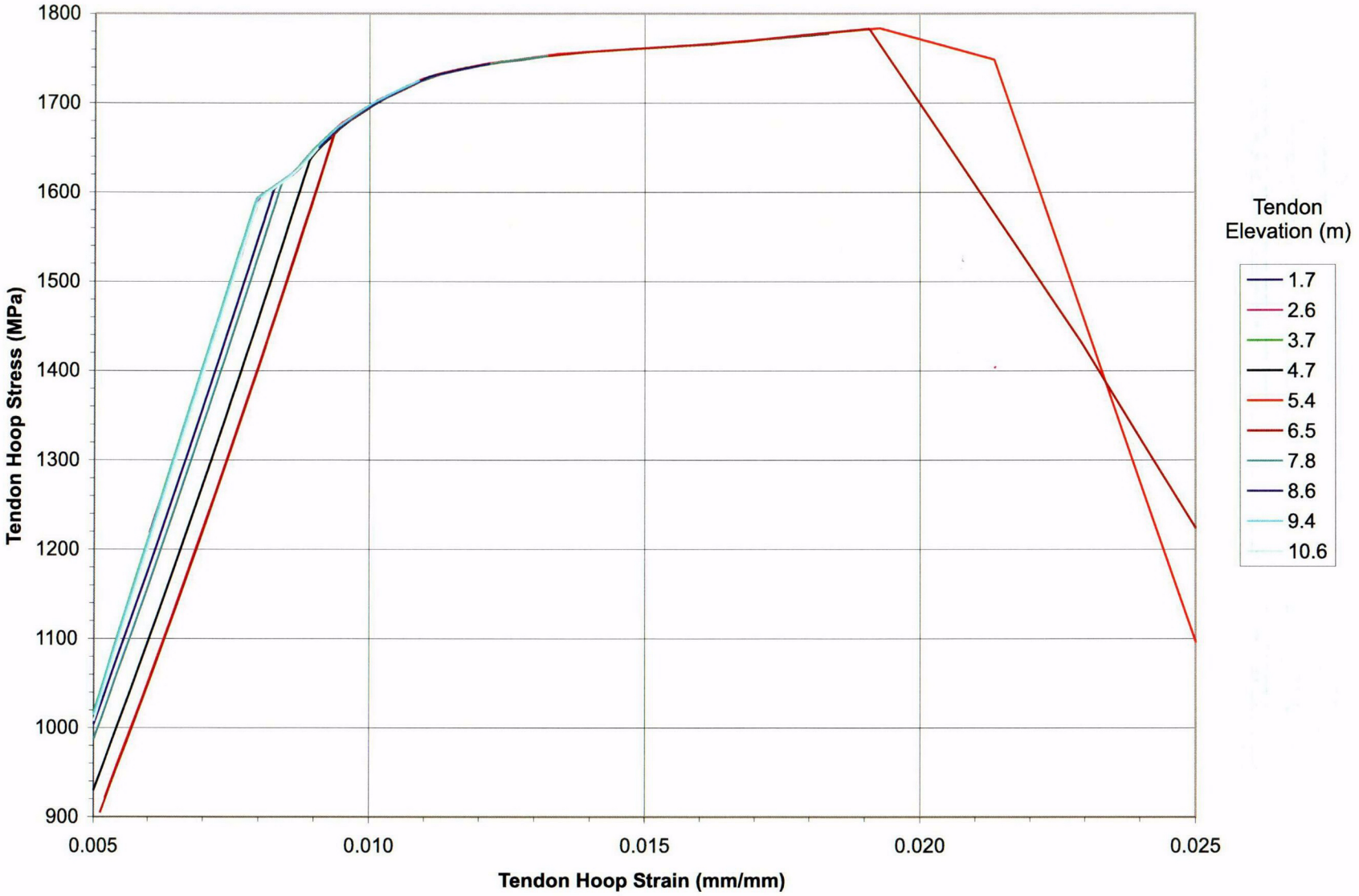

Figure 9-32. PCCV SFMT, 3D Global Shell Model-Hoop Tendon Stress Versus Strain History, Tendon History at 0 Degrees Azimuth, P = 1.389 MPa, 3.53 Pd

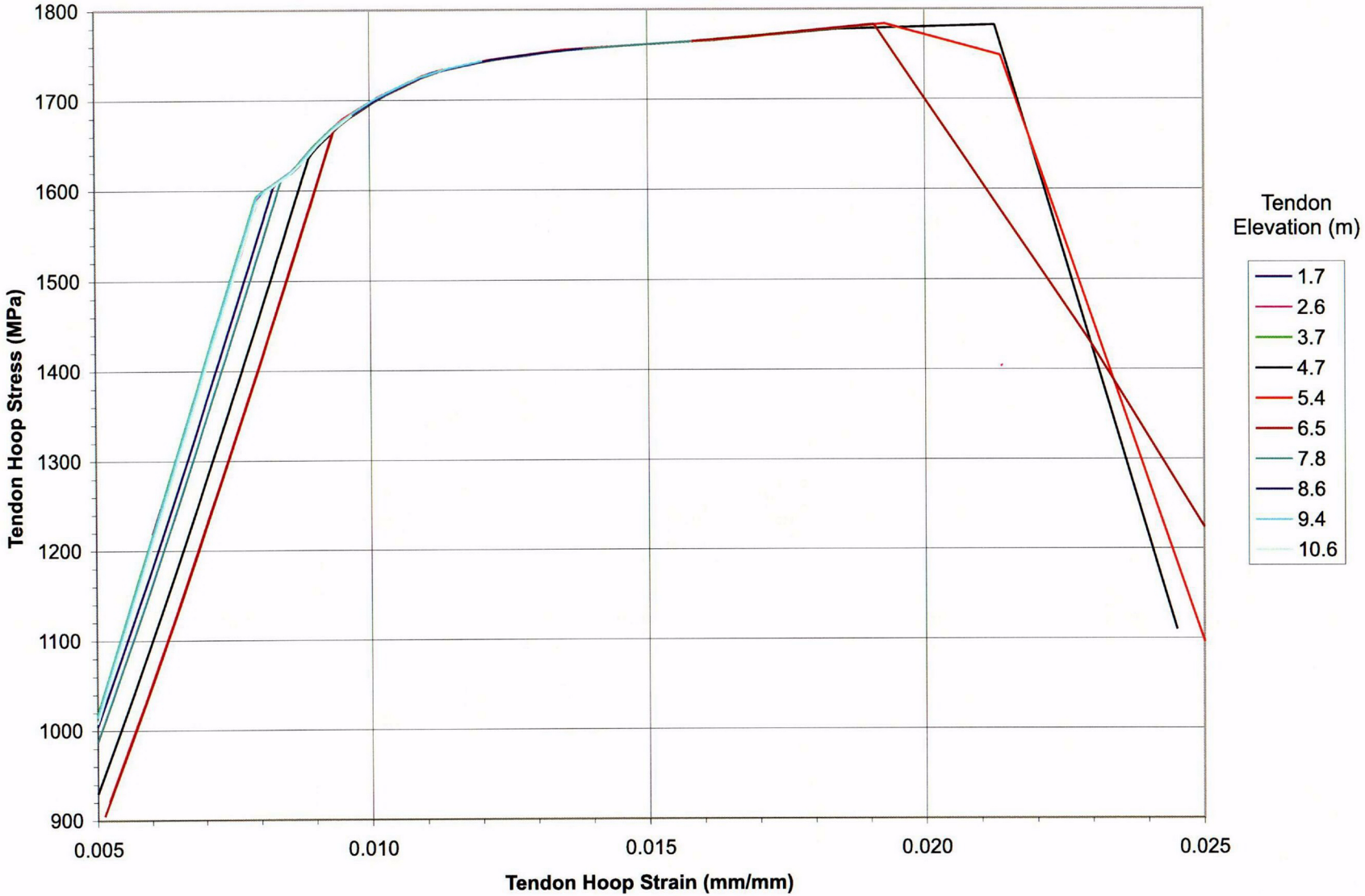

Figure 9-33. PCCV SFMT, 3D Global Shell Model-Hoop Tendon Stress Versus Strain History, Tendon History at 0 Degrees Azimuth, P = 1.404 MPa, 3.57 Pd

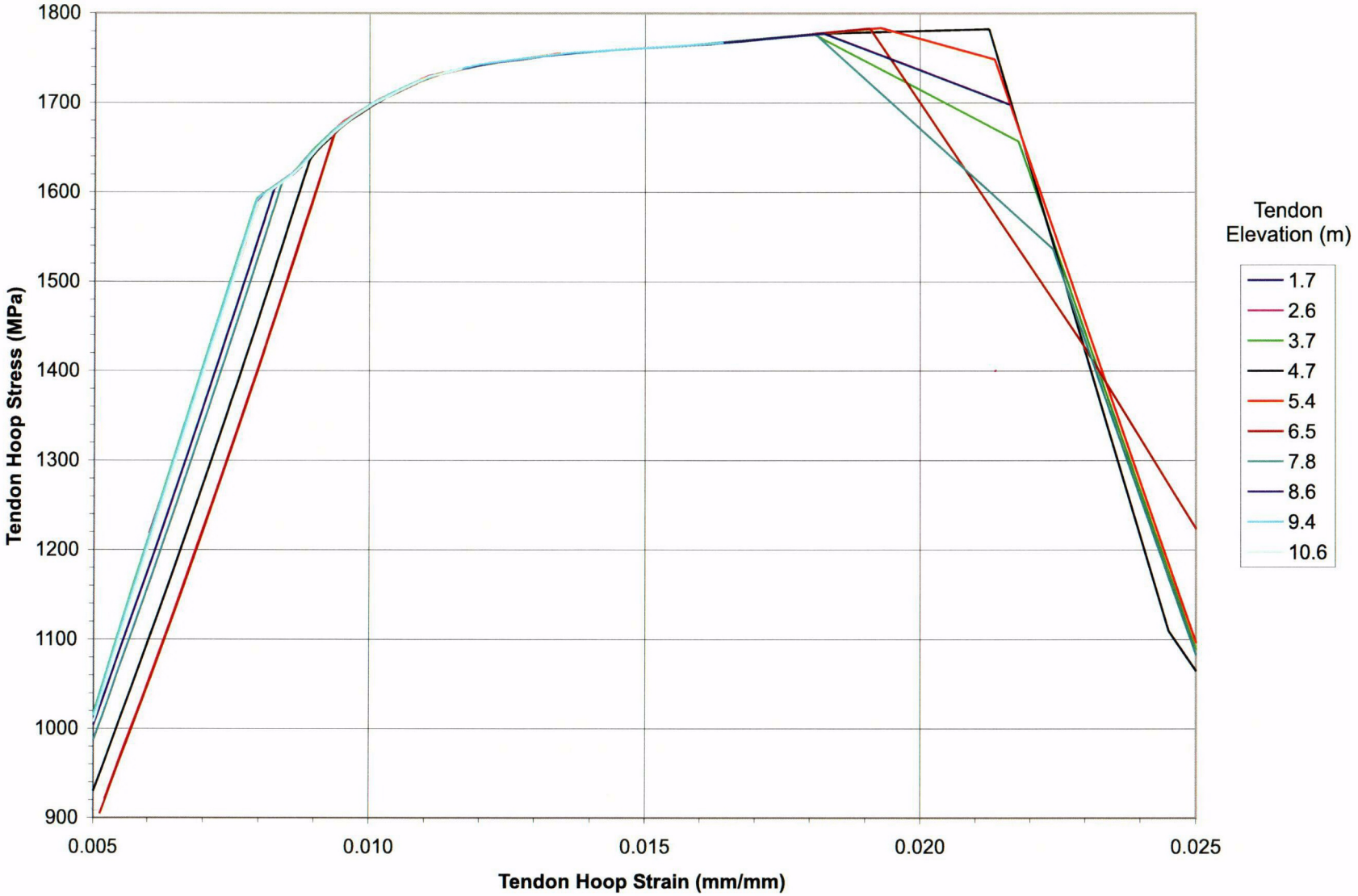

Figure 9-34. PCCV SFMT, 3D Global Shell Model-Hoop Tendon Stress Versus Strain History, Tendon History at 0 Degrees Azimuth, P = 1.436 MPa, 3.65 Pd

C278

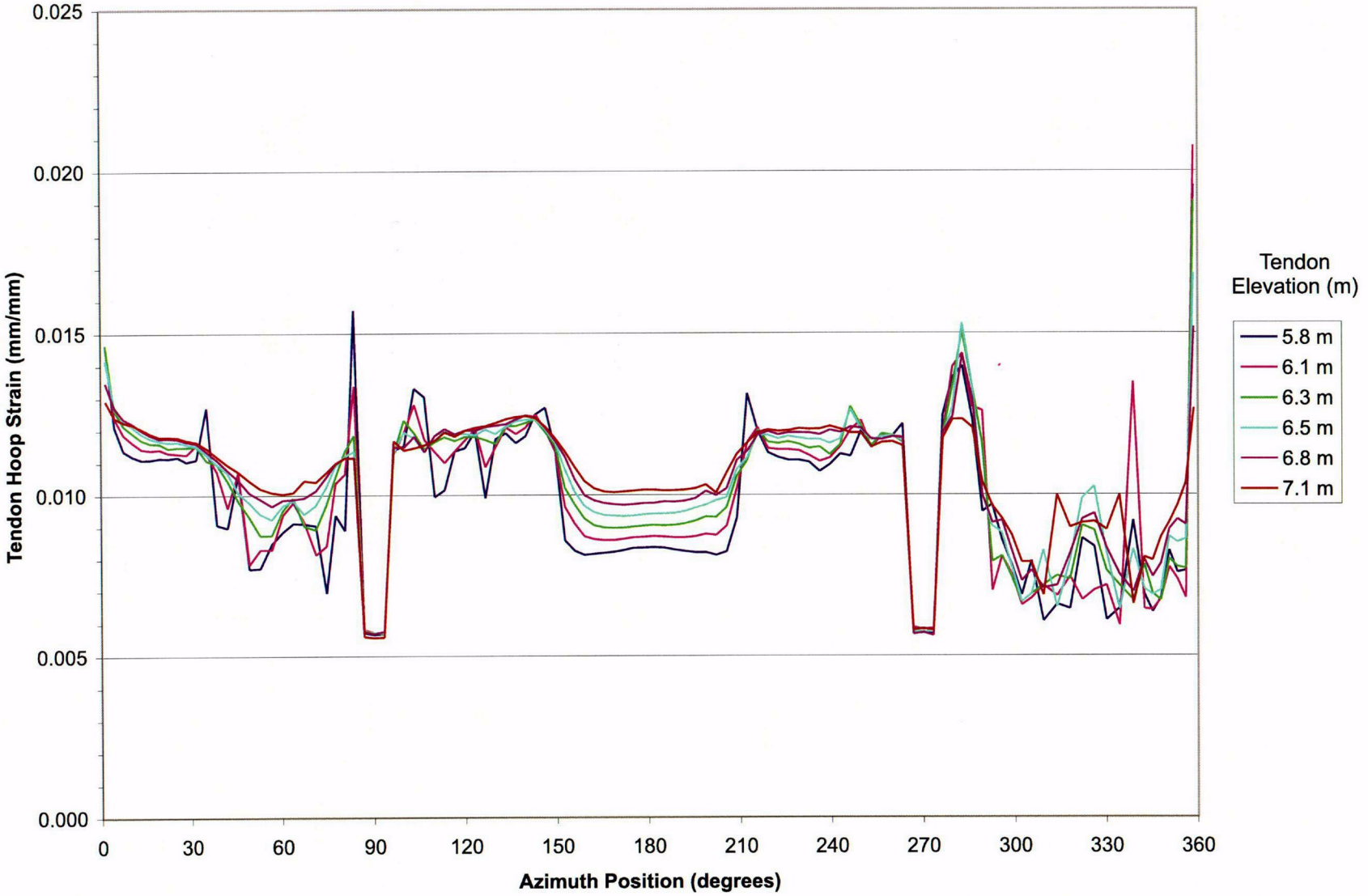

Figure 9-35. PCCV SFMT, 3D Global Shell Model-Hoop Tendon Strain Profile, Tendon History, P =1.357 MPa, 3.45 Pd

C279

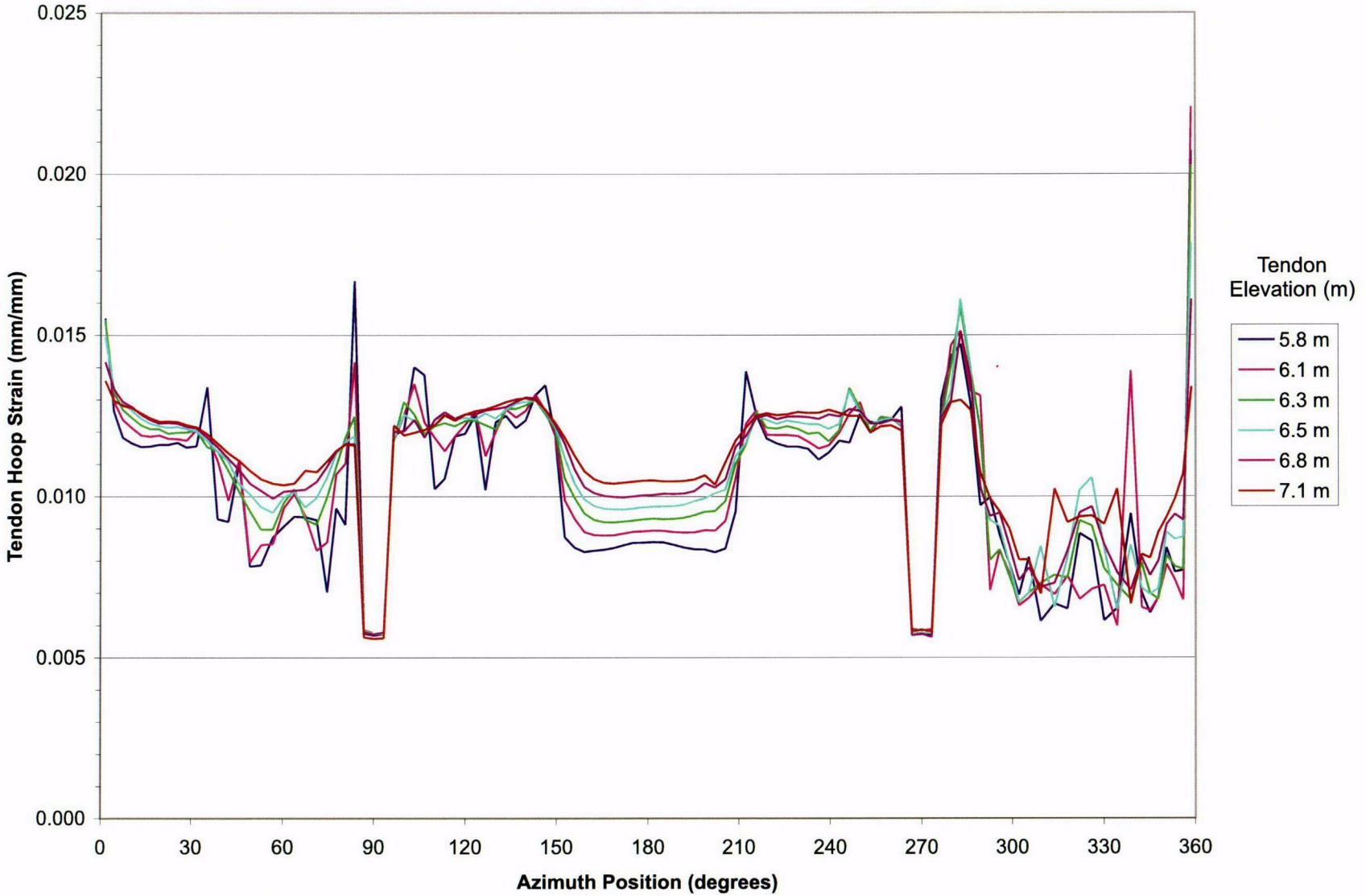

Figure 9-36. PCCV SFMT, 3D Global Shell Model-Hoop Tendon Strain Profile, Tendon History, P =1.366 MPa, 3.47 Pd

C279A

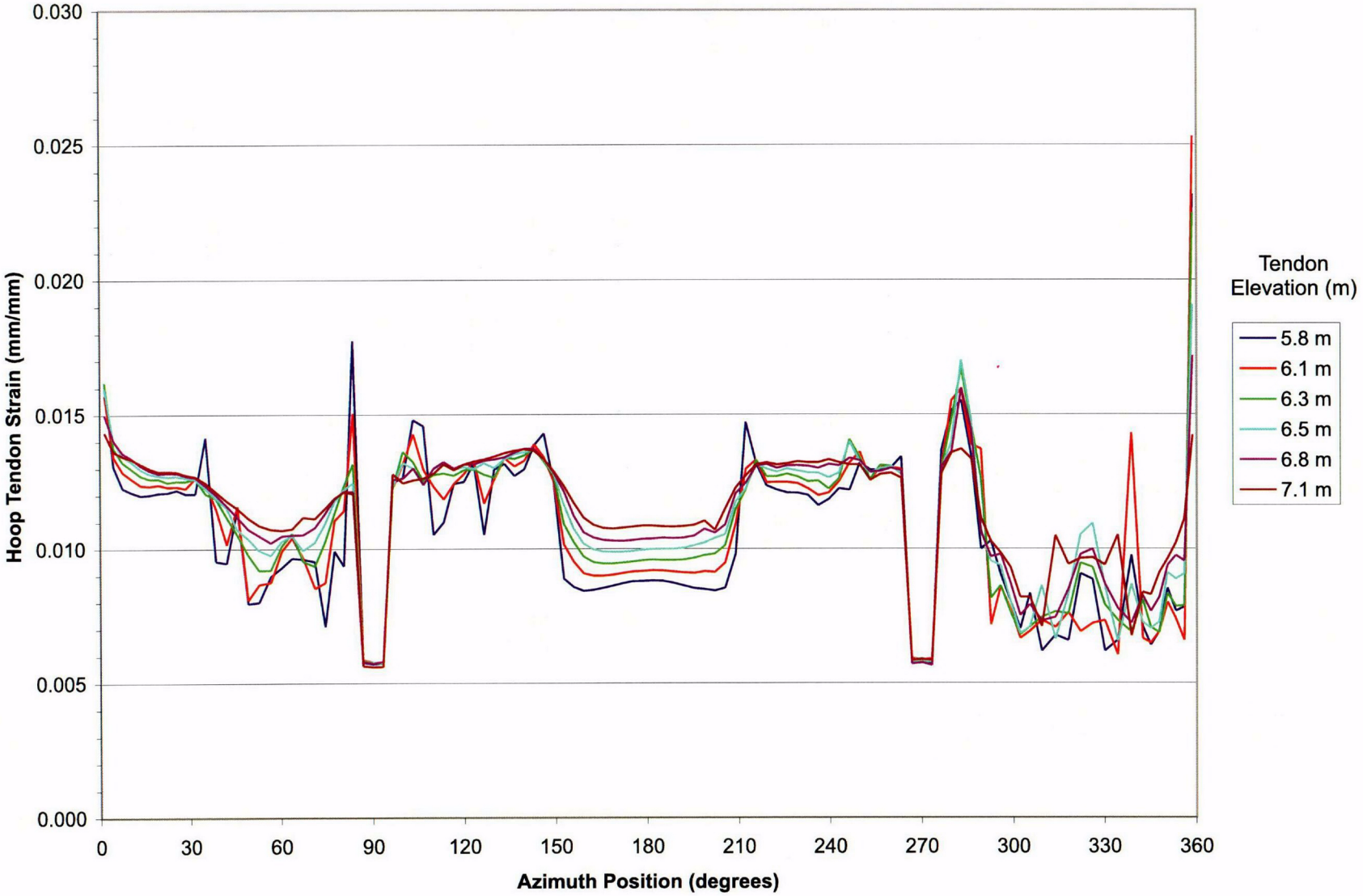

Figure 9-37. PCCV SFMT, 3D Global Shell Model-Hoop Tendon Strain Profile, Tendon History, P = 1.373 MPa, 3.49 Pd

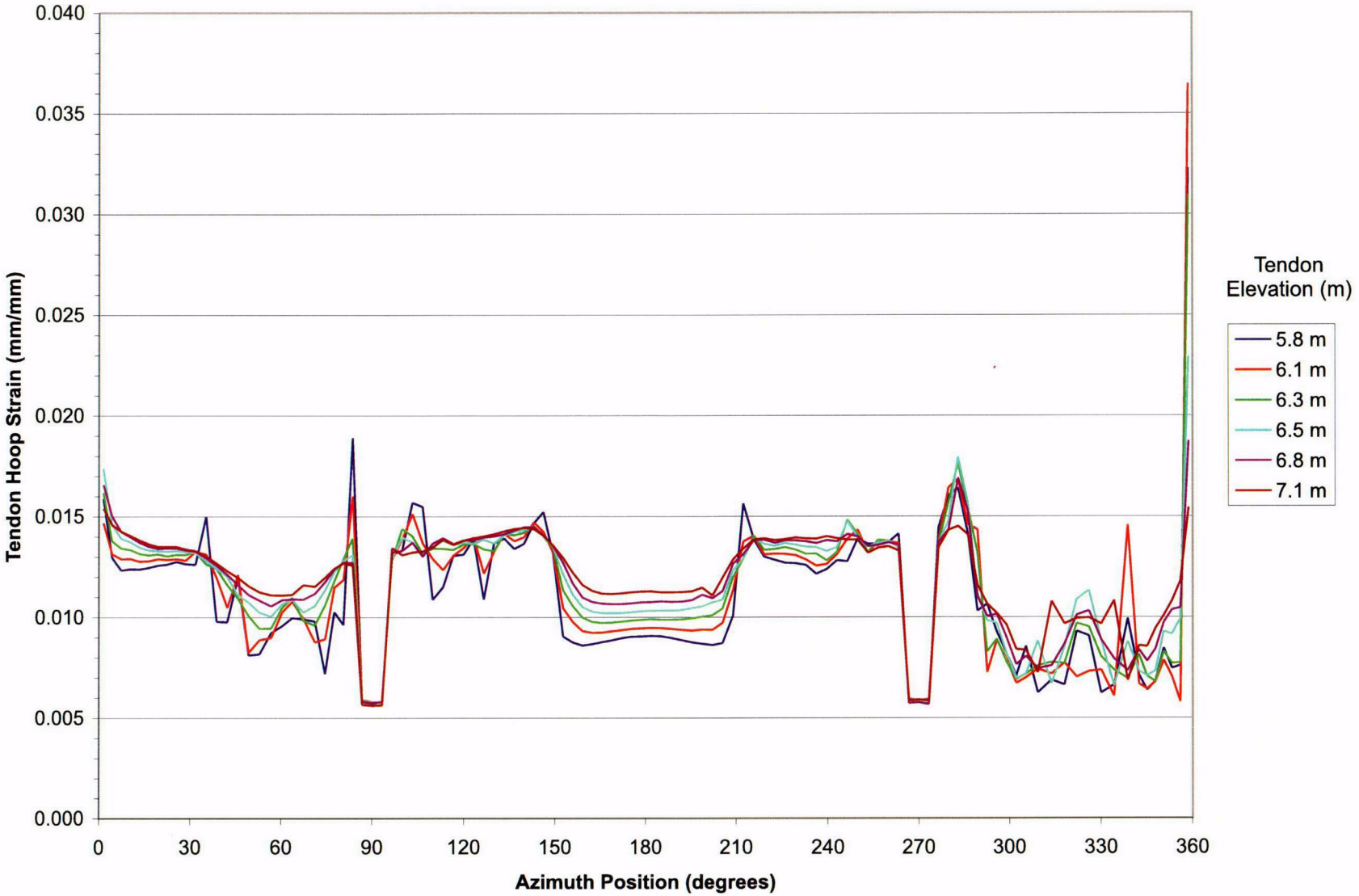

Figure 9-38. PCCV SFMT, 3D Global Shell Model-Hoop Tendon Strain Profile, Tendon History, P = 1.381 MPa, 3.51 Pd

C281

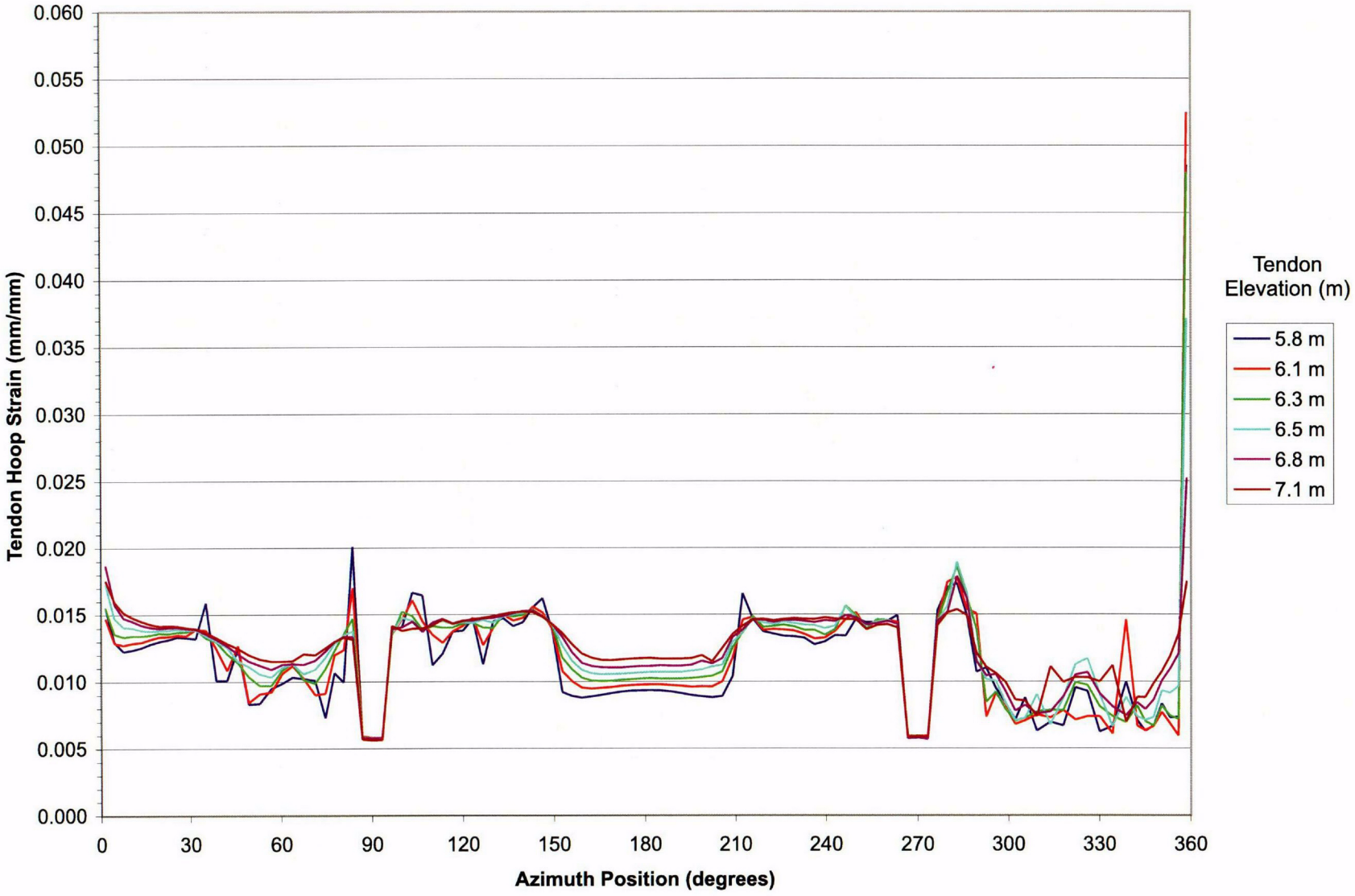

Figure 9-39. PCCV SFMT, 3D Global Shell Model-Hoop Tendon Strain Profile, Tendon History, P = 1.389 MPa, 3.53 Pd

C282

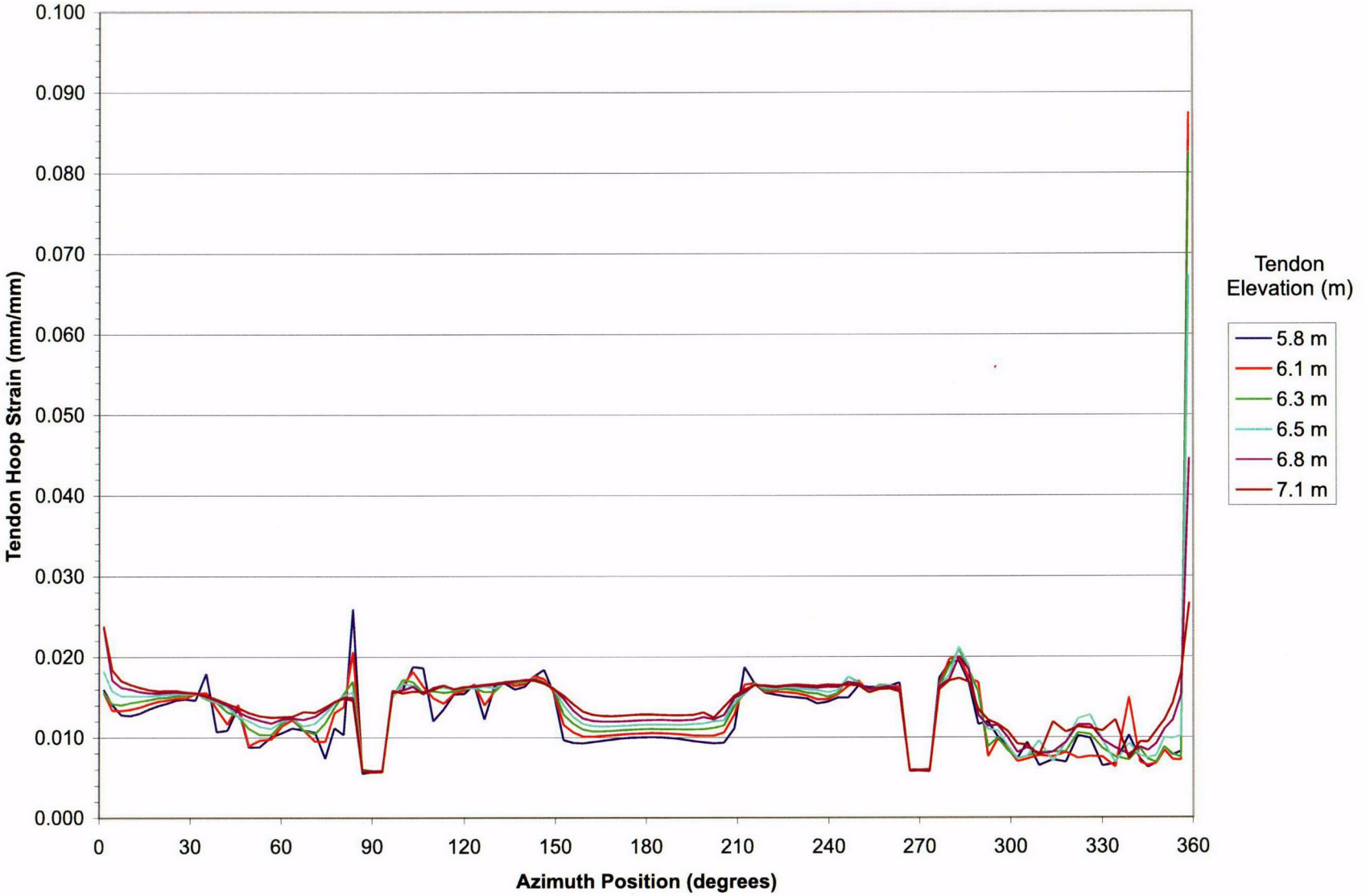

Figure 9-40. PCCV SFMT, 3D Global Shell Model-Hoop Tendon Strain Profile, Tendon History, P = 1.404 MPa, 3.57 Pd

C283

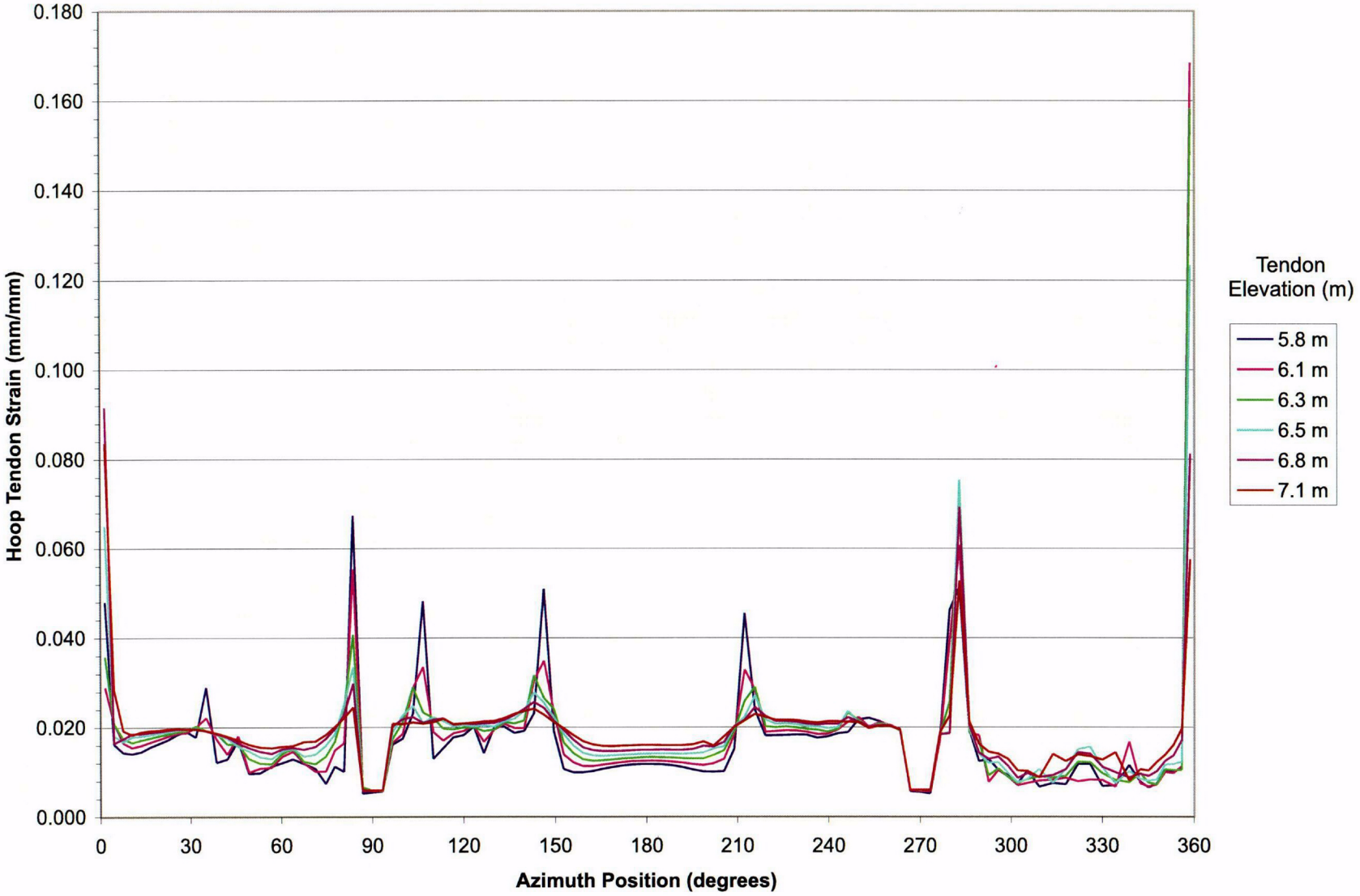

Figure 9-41. PCCV SFMT, 3D Global Shell Model-Hoop Tendon Strain Profile, Tendon History, P = 1.436 MPa, 3.65 Pd

C284

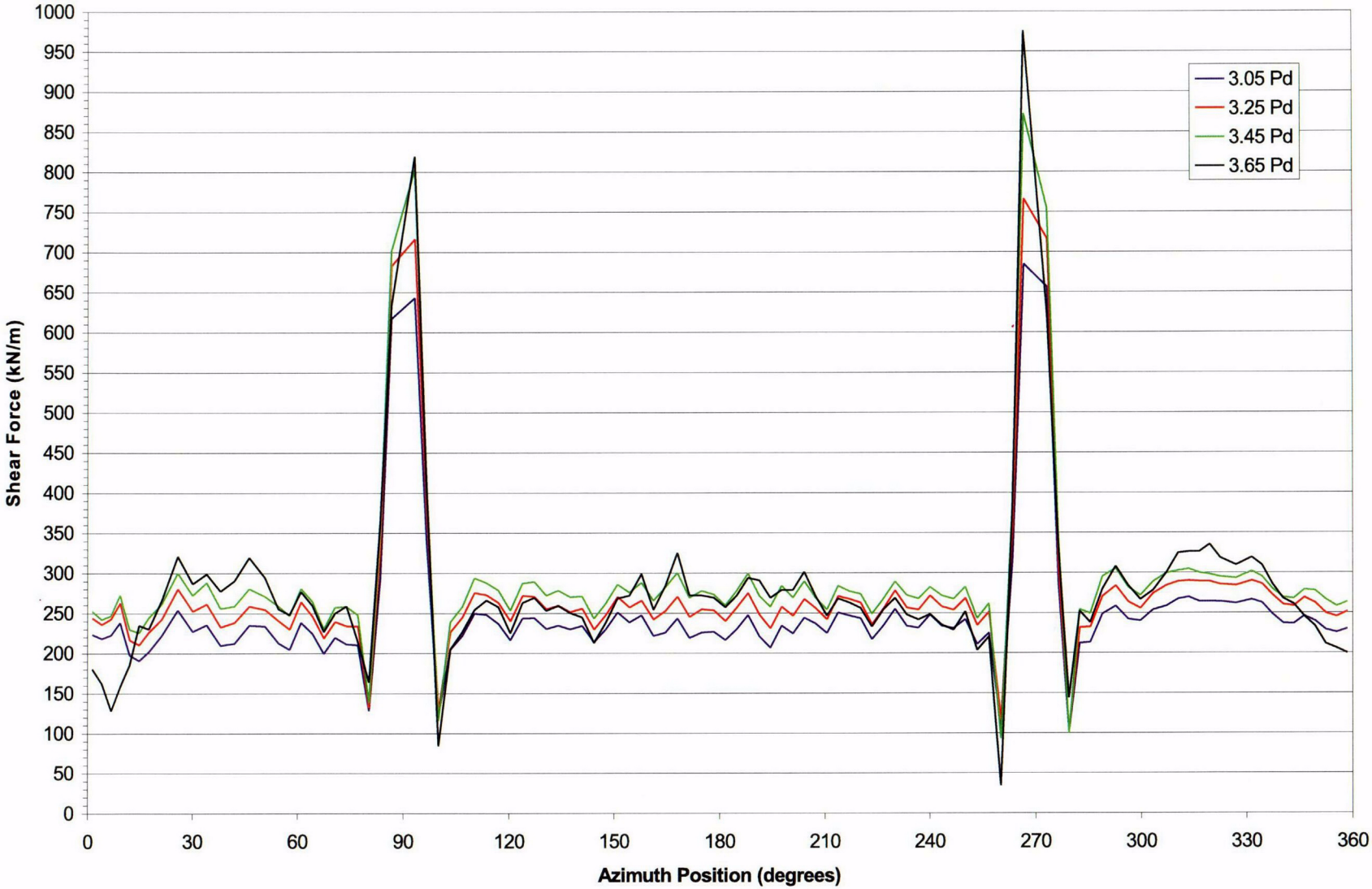

Figure 9-42. PCCV SFMT, 3D Global Shell Model - Cylinder Shear Profile 1 m Above Basemat

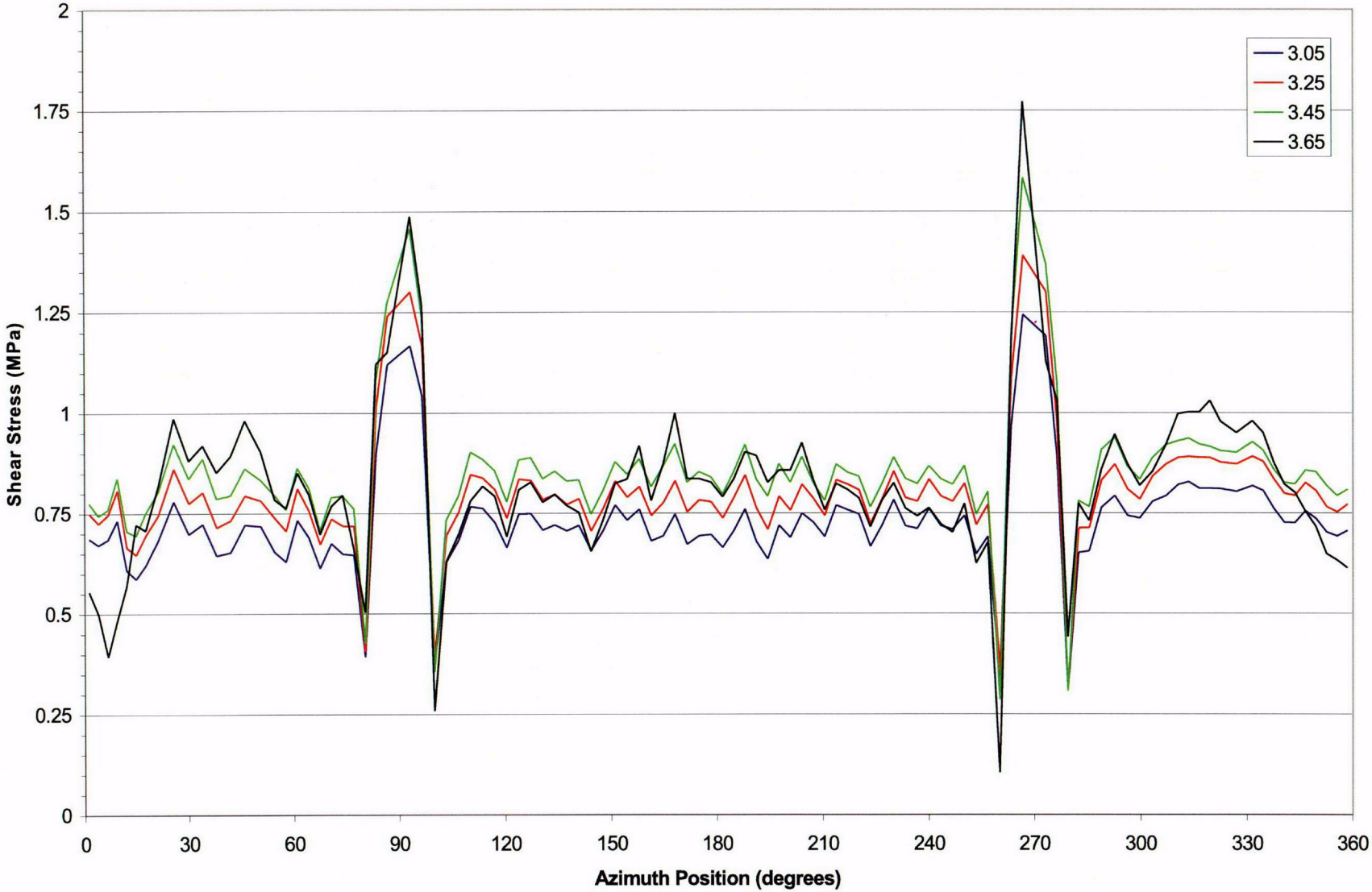

Figure 9-43. PCCV SFMT, 3D Global Shell Model - Cylinder Shear Profile 1 m Above Basemat

C286

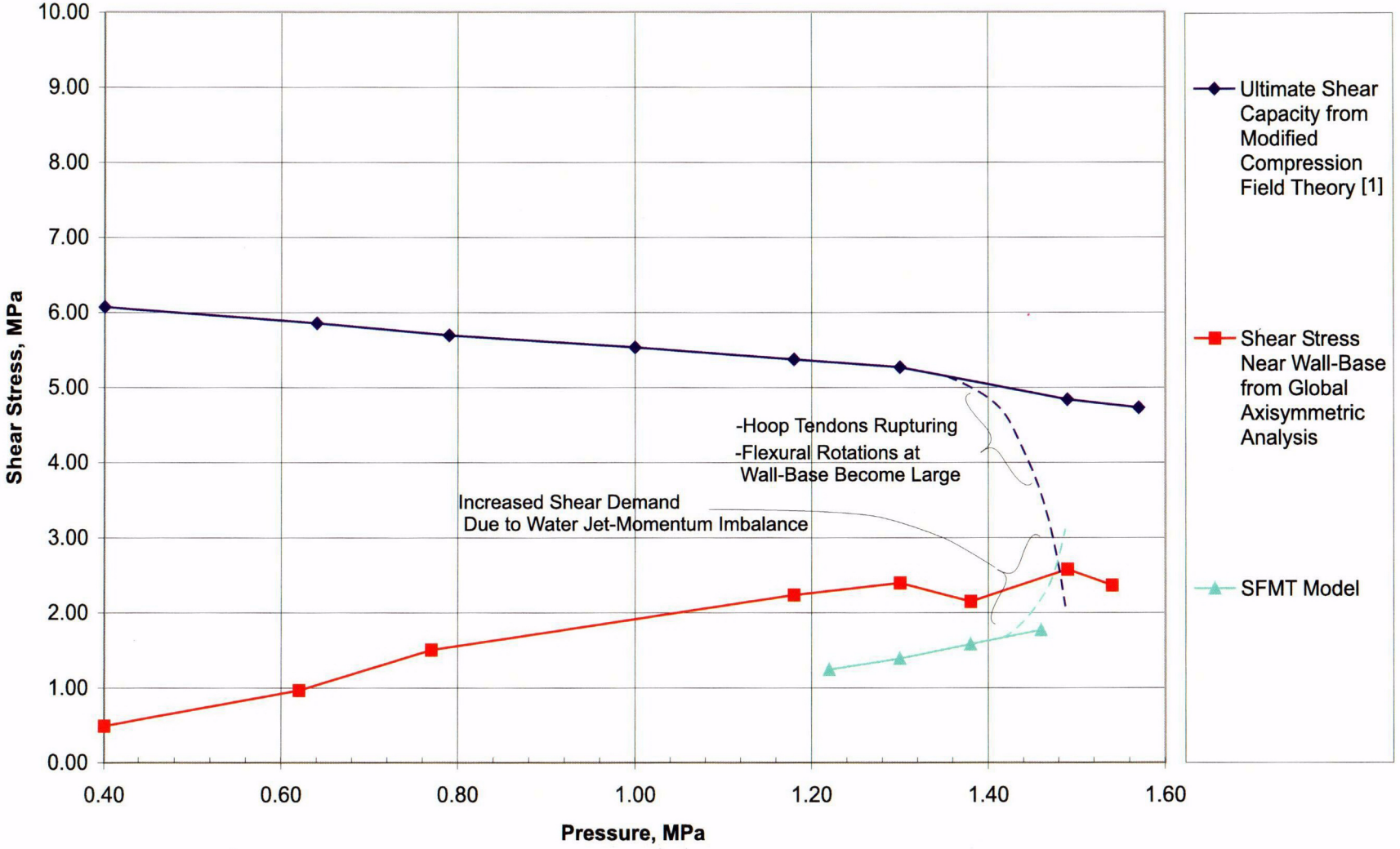

Figure 9-44. PCCV Wall-Base Shear Strength from Modified Compression Field Theory Compared to Shear Demand from the Global Analysis Model [1] and the SFMT Model

C287

10.0 CONCLUSIONS AND LESSONS LEARNED

10.1 Conclusions of Post-Test Analytical Studies of the PCCV LST

As part of the NUPEC and NRC-sponsored Containment Research Program conducted at Sandia National Laboratories, a 1:4 scale model of a prestressed concrete containment vessel (PCCV) has been constructed, pressure tested to failure, and studied with preliminary, pretest, and post-test analytical evaluations. All analyses were performed using the nonlinear concrete constitutive model, ANACAP-U, in conjunction with the ABAQUS general purpose finite element code. The documentation of post-test analysis work herein has included: a final series of pretest analyses (performed to support test operations and account for information, such as tendon prestress levels, learned in the final months prior to the test); a comprehensive set of comparisons of test measurements to pretest analyses; review, model modification, and re-analysis of pretest analytical models to incorporate as-built conditions or improve levels of correlation with the test; and development and study of liner seam/rat-hole detailed models to gain insight on the behavior mechanisms surrounding the liner tears that occurred in the test. Review and standardization of measurements taken during the LST have also been conducted.

The effects and phenomena studied in the "data correction" effort were temperature, rigid body motion of the model, and strain localization. Temperature, as a direct influence on structure strains and displacements and as a secondary influence on voltage readouts of strain gages, was corrected for, the former being calibrated by direct observation of model response during the spring and summer of 2000, and the latter being calibrated by formulae provided by the gage manufacturer. To correct for either phenomena, a temperature mapping algorithm based on interpolation between the matrix of temperature gages, was developed. Additional correction was considered for rebar gages, but was ultimately left up to end users to apply as deemed appropriate. Without such correction, however, users should note that the rebar gage measurements tend to overpredict the apparent engineering strain, especially in the strain range just past initial yield, i.e. between $\varepsilon = 0.002$ and $\varepsilon = 0.015$. The cause for this is area reduction associated with grinding for gage-preparation.

The overall conclusions from the comparisons of the pretest analyses with the test data are as follows:

- Radial displacements were well predicted by global axisymmetric analysis, but dome and overall vertical displacements were significantly overpredicted.
- Measured basemat uplift was much smaller than predicted, but this is judged to be an artifact of how this quantity was measured.
- Wall-base juncture behavior, including many rebar and liner strain measurements, was well predicted by the detailed wall-base juncture (axisymmetric) modeling.
- The maximum pressure, 1.30 MPa (187.9 psig) or $3.30P_d$, which was primarily a function of the onset of global yielding, was very close to the prediction of liner tearing at the equipment hatch at a pressure of 1.28 MPa (185 psi), although the predicted tears did not occur. The strains occurring in the test model at the primary tear prediction location were very small.
- An initial small leak occurred at $2.5P_d$ that was not predicted by analysis, but this may be due to defects associated with weld seam repair.
- The average radial displacement of 23mm, equivalent to an average hoop strain of 0.0040, was well predicted by global analysis.
- The maximum radial displacement at the E/H of 29mm, equivalent to a hoop strain of 0.0054, was well predicted by 3DCM model, but prediction of some displacements at other azimuths, like the buttresses, was poorly predicted by 3DCM model.
- Tendon stress distribution simulated by analysis at start of LST shows fair agreement with measurements, implying that the angular friction and anchor set modeling assumptions at start of test were reasonable.
- Hoop tendon stress distributions during pressurization showed poor agreement with the pretest analysis. In particular, the gages interior from the ends were underpredicted and the anchor forces were overpredicted.
- Cylinder hoop tendon data shows evidence that angular friction forces were overcome by differential tendon forces resulting in the tendons sliding, relative to the ducts, during pressurization. The measurements indicate that the shape of the tendon stress profile completely changes during pressurization. The increase in tendon

strain, which is greater than the corresponding cylinder wall hoop strain, implies that portions of the tendons are slipping in order for higher deformation at other azimuths to be accommodated.

- As with the hoop tendons, there was about 8% to 10% loss in vertical tendon force between the initial prestressing and the start of the LST caused by long term effects and by the SFT and SIT. Only one tendon, V85 showed significant friction losses below the springline, and the other two gaged vertical tendons showed only about half of the friction loss in the dome than what was assumed by designers and incorporated in analysis.

Initial post-test analyses were run with ABAQUS Version 5.8-15. When ABAQUS Version 5.8-18 was used in post-test analysis, a significant program bug was found in 5.8-18 (and 5.8-21) related to the use of "Prestress Hold" and small deflection theory. (Small deflection theory was used in conjunction with the tendon friction modeling strategy adopted for the curved portions of tendons.) The bug was finally resolved by ceasing to use the "Prestress Hold" option. Now Version 5.8-18 was used for all post-test analyses, but without "prestress hold" - by increasing the prestress to account for elastic shortening. The conclusions reached about post-test global axisymmetric analyses are summarized below.

- Uplift and dome displacement simulations were significantly improved by redistributing soil basemat springs according to tributary area, and by thickening the dome meridional tendon representation due to the rectilinear "hairpin" layout.
- Predictions were also improved by using no vertical tendon friction in the cylinder.
- Analysis using ABAQUS should not use the Prestress Hold option.

The important conclusions from comparing the 3DCM model pretest analysis to the LST follow:

a. The 3DCM model predicted significantly larger radial deformations than the test measurements and more than the axisymmetric analysis.
b. At pressures lower than $3.0P_d$, the buttresses (90/and 270/) bulge out radially more than most other azimuths. This trend reverses itself beyond $3.0P_d$, but at $P < 3.0P_d$ the trend is at odds with test observation.
c. While the 3DCM model did provide a good simulation of the distribution of tendon stress at the test's initial conditions, as pressure increased it is clear that very different stress redistribution occurred in the tendons than was simulated by the analysis.

The first change introduced for post-test 3DCM modeling was that the buttresses above and below the 3DCM model boundaries were given vertical beam stiffnesses that was not accounted for in the pretest analysis. The next and only other modeling assumption found to be at significant variance with observed test behavior was the tendon friction modeling. Two important observations were made about the hoop tendon measurements as pressure increases:

1. When pressure reaches the "Pressure to overcome prestress," P = 0.59 MPa, tendon stress distributions change from the classical angular friction design assumption to approximately uniform distribution; toward the end of the test, some tendon interior forces slightly exceed the force at the anchor.
2. The "apparent strain" increases in the tendons corresponding to the force/strain gage readings are significantly larger than the strain that corresponds purely to radial expansion. This can only be explained by force redistribution associated with sliding.

These observations led to changes and studies of the tendon friction modeling. The final analyses performed were:

Run 6. Apply Prestress. Then by using the ABAQUS *MODEL CHANGE capability, fix the tendon nodes at their initially deformed position relative to the concrete. In other words, start from classical design prestress with friction and then grout (bond) the tendons.

Run 7. Perform Run #5 (the Run with only the buttress springs added) up to $P = 1.5P_d$ (0.59 MPa), then "Model Change" all friction elements to non-friction elements (truss ties aligned perpendicular to the tendons. In other words, at $P = 1.5P_d$, perfectly "grease" (unbond) the tendons.

Run 9. After prestress, keep the initial friction elements, but add a new set of friction elements in the reverse orientation so that if points on the tendon move relative to concrete in the reverse direction from that of initial prestress, they will experience reverse direction friction.

The tendon friction simulation runs 6, 7, 9 showed progressively better agreement with test measurements, with Run 9 showing quite good agreement at the anchors and at most points interior to the tendon ends. The results of Run 9 were used for driving the M/S (and estimated F/W) penetrations post-test analysis. On tendon friction behavior, the test measurements and analytical evidence support the conclusion that tendon friction is important to the tendon behavior, but traditional friction design formulas that predict tendon stress distribution begin to break down once pressurization exceeds the pressure that "overcomes" prestress (in this case, roughly 1.5Pd). The coefficient of angular friction appears to lessen to allow sliding and force redistribution as the vessel expands, but more importantly, some parts of the tendon are forced to reverse direction of travel relative to the duct, reverse it from the direction of travel experienced during prestressing. Under this action, angular friction properties probably still hold, but perhaps with a reduced coefficient, and the direction of friction changes sign from that assumed in a design calculation.

Liner strains measured in the vicinity of the E/H penetration collar were much lower than predicted by pretest analysis. Two hypotheses were developed and subsequently proven by the post-test analyses. Post-test analysis showed that by preventing relative slip between liner and concrete, the overall behavior of the system (concrete strains, tendon strains, liner strains away from the hatch) remained the same, but the elevated strains close to the collar were eliminated. This supports a conclusion that the liner in the E/H area had a high degree of bond-friction with concrete, preventing slippage of the liner relative to the concrete; relative slippage is required for elevated strains to develop near local discontinuities like T-anchors and stiffeners. In a final case, directed cracks were introduced to one row of elements, and a discrete crack was formed by adding double rows of nodes along an assumed crack line. This was found to create a liner elevated strain phenomenon. This supports a conclusion that formation of a major crack near the edge of the E/H embossment further concentrated the liner strains at the edge of the embossment. The mild strain concentration coincides, in location, with rat-hole weld seam details, and in the LST, numerous tears occurred at these details. Based on results of detailed liner rat-hole (weld-seam) analysis, the additional strain concentration associated with these details was found to be enough to make a tear prediction at the edge of the embossment. This shows that with discrete crack modeling and local rat-hole modeling, a liner tear could have been predicted to occur as early as $2.8P_d$. Based on the evidence provided by liner strain gages and by acoustic monitoring, one of the tears along this embossment edge may have even occurred as early as $2.5P_d$. A higher strain prediction might be possible if a discrete crack (separate rows of nodes) were propagated all the way through the concrete wall, but this would require a change in rebar modeling strategy - one that is probably not practical even for very detailed analytical evaluations of containments.

The Mainsteam (M/S) and Feedwater (F/W) Penetration "hot spots" (both analysis and LST observations) occurred near the vertical T-anchor terminations and near the thickened insert plate surrounding the penetration group, e.g. at the 3 o'clock and 9 o'clock positions. For the post-test analysis effort no changes to the M/S model were found to be necessary, other than updating the applied displacement versus pressure histories, which were obtained from 3DCM post-test model 9. The M/S and F/W locations were well instrumented with liner strain gages. These provided the following observations and conclusions relevant to response prediction for containment penetrations.

- Many of the highest strains recorded during the LST were near the M/S and the F/W.
- There was a wide variation in peak strain data, even at locations which were theoretically identical in geometry; factors contributing to these differences: slight variations in liner thickness (due to manufacturing and weld repair grinding), gage position relative to the collar/weld, material properties (including welding heat effects), etc.
- The highest strain measurements can, but do not always, correspond to tear locations. Examples supporting this are: 1) a gage near the F/W tear shows evidence of rising strain prior to tear occurrence, then starting at $2.9P_d$, declining strain due to the stress relief caused by the tear; a gage located near the crack tip, on the other hand, showed quite low strain up to $3.1P_d$ and then a sudden jump. This supports a hypothesis that this tear initiated at a pressure of $2.9P_d$ at about the 7:30 o'clock position (mid-point of the tear) and then between $2.9P_d$ and $3.1P_d$, the tear ran around the perimeter of the thickened collar and up to the 9 o'clock position.

Comparisons of analysis to the M/S and F/W liner strain gages show that the post-test analysis of the M/S penetrations captured the strains measured in the LST quite well for both the M/S and F/W penetrations.

Post-test liner seam studies led to the following conclusions and insights on liner seam/rat-hole modeling and behavior:

- By comparison with strain gage measurements and post-test liner tear observations, some of the finite element weld seam meshes capture the strain concentrations in and around the rat-holes and liner welds very well.
- Because of competing mechanisms (between the weld zone and the ends of stiffeners) making yield and ultimate strength adjustments to the HAZ material properties appears to be justified and necessary to correctly predict strain concentration location and intensity.
- Including back-up bars, nominal geometric properties and best estimate material properties, is the best way to predict behavior of defect-free rat-hole/weld-seam details, as probably occurred in the PCCV model at locations such as D7 and J5; however, even without back-up bars, also provided reasonable correlation with gages at these locations.
- A case with severe (~40%) amounts of thinning provided best simulation of behavior of tears with severe liner thinning (due to weld repair grinding as reported in [7]) and back-up bars absent; these conditions existed at Tears 7, 8, 10, 12, 13, 14, 15, and 16.
- A case specifically representing the Tear 16 detail provided reasonable simulation of the tears that occurred with back-up bars present, namely, Tears 1, 2, 6, 9, 11, and 16. The severity of the strain at this case also shows that a tear ($\varepsilon_{eff} > 20\%$) at the geometry simulated would have been predicted to occur as early as $3.0P_d$.
- If a section of liner with a rat-hole/liner-seam such as at Tears 7, 12, 13, 15 is subjected to elevated strain (i.e. strain across the liner model that is larger than free-field strain) a tear even earlier than $3.0P_d$ can be justified. In practice, such a prediction could be approximated using a strain concentration factor approach. The strain concentration factors (K = peak ε_{eff} divided by global ε_{hoop}) implied by this liner seam study are as follows: K = 48 (tear at Stiffener End, no back-up bar); K = 45 (tear at Stiffener End, with back-up bar); K = 59 (tear at HAZ, no back-up bar, and 40% thickness reduction due to grinding); K = 91 (tear at Tear 16, if a short segment of horiz. weld seam back-up bar is missing)
- Using a model of the rat-hole/seam locations without defects, such as location D-7, showed that liner tears still would have developed by pressure of $3.4P_d$, so liner tearing and leakage would still have been the failure mode (for quasi-static pressurization) even in the absence of liner welding irregularities.

10.2 Summary of Lessons Learned and Guidelines for Prestressed Concrete Containment Analysis

The 1:4 Scale PCCV test has, as with other containment pressurization tests, shown that the driving response quantity which leads to limit state of the vessel is the radial expansion of the cylinder. This aspect of response must be predicted correctly in order to reasonably predict vessel capacity and predict, at least approximately, the many other local aspects of response (local liner strains, etc.) that are driven by the cylinder expansion. With this test, as with the 1:6 Scale RCCV model [9], many competing strain concentrations occur around the midheight of the cylinder. Although it is difficult to predict which local liner detail will tear first, and although some particular response quantities, like basemat uplift, were not predicted exactly by the ANATECH/SNL pretest analysis of the PCCV model, the radial expansion of the cylinder was predicted very accurately.

A response mechanism which also appears to have been well predicted was cylinder wall-base flexure and shear and this is another mechanism that, if predicted grossly incorrectly, could lead to very erroneous pressure capacity/failure mode conclusions.

The local analyses and 3DCM analyses provided additional insights into local behaviors, albeit with some inaccuracies that have been identified herein – in particular, tendon friction and liner friction modeling considerations. Thus, in the author's opinion, the combination of the pretest analysis [1] and post-test analysis conducted for the PCCV provides a good road map and example for conducting a detailed analytical evaluation of a containment vessel. As followed in this road map, therefore, a detailed containment evaluation should consist of the following steps. The steps are listed in order of descending priority and in order of increasing complexity and accuracy. The minimum requirement for a containment overpressure evaluation should certainly be a robust axisymmetric analysis, Step 4 shown below:

1. Review drawings, geometry, and material property information
2. Based on what is known about containment behaviors from the last two decades of research (SNL/USNRC, EPRI, and international containment research), list the potential failure modes and failure mechanisms that are possible for the structure. (This was done in [1].)
3. Idealize material property information. This should include digitization of concrete, liner, rebar, and tendon stress-strain curves. For tendons, stress-strain input should be the net axial stress and strain, adjusting for the wrap angle of the strands, if applicable.
4. Develop and analyze axisymmetric analysis model. This model can be relatively coarse in the cylinder wall and dome, but should be fine and detailed at the wall-basemat juncture. The methods and assumptions described in the post-test analyses of this report can be used for guidance.
5. Develop and analyze a 3D model that captures the 3D aspects of the cylinder deformed shape. This could be either a 3D model of the entire structure, or a ring model of a portion of the cylinder. The ring idea was used here, because of the difficulty to model individual tendons with friction simulation for a full global 3D model. Various lessons learned on tendon modeling have been identified in this report and are highlighted again here. (It should be noted that a 3D "slice" model is not adequate for capturing the non-asixymmetric aspects of the structure which affect the response, i.e., the positions of the penetrations, etc.)
6. Develop and analyze local models as needed to predict liner tearing.

Below are some other "lessons learned" about axisymmetric analysis:

- Comparisons between the test and the axisymmetric analysis show that assuming no friction along the straight portion of tendon and smaller friction in the dome than designers calculate will provide improved simulation of the vertical tendon behavior.
- Uplift and dome displacement predictions were significantly improved by redistributing soil basemat springs according to tributary area, by allowing up to 10 psi tensile "stick" under the basemat, and by thickening the dome meridional tendon representation due to the rectilinear "hairpin" layout.
- Analysis using ABAQUS should not use the "Prestress Hold" option.
- The best calculation methods that can now be recommended for tendon friction modeling are, in descending order of preference,
  1) an advanced contact friction surface between the tendons and the concrete (not manageable for the current problem size and complexity),
  2) Pre-set friction ties applied in one direction during prestressing and then added in the other direction during pressurization (3DCM Run #9), and
  3) if neither of these methods are practical within the scope of the calculation, it is best to start with an "average" stress level (using a friction loss design formula), but assume uniform stress distribution in the tendons throughout pressurization, i.e., an unbonded tendon assumption, and finally
  4) same as 3, but using a bonded tendon assumption. (It should be recognized for method 4, however, that this can lead to a premature prediction of tendon rupture, because the tendon strain increments during pressurization will match the hoop strain increments of the vessel wall one-to-one, and this is not what was observed to occur during the PCCV LST.)

11.0 REFERENCES

1. Dameron, R. A., et al. 2000. *Pretest Analysis of a 1:4-Scale Prestressed Concrete Containment Vessel Model*, NUREG/CR-6685, SAND2000-2093. Albuquerque, NM: Sandia National Laboratories.

2. Dameron, R. A., Rashid, Y. R., Luk, V. K. and Hessheimer, M. F. 1997. "Preliminary Analysis of a 1:4 Scale Prestressed Concrete Containment Vessel Model," in *Proceedings of the 14th International Conference on Structural Mechanics in Reactor Technology,* Vol. 5, pp 89-96, Lyon France.

3. Luk, V. K. 2000. *Pretest Round Robin Analyses of a Prestressed Concrete Containment Vessel Model.* NUREG/CR-6678, SAND00-1535. Albuquerque, NM: Sandia National Laboratories.

4. *ANACAP-U User's Manual*, Version 2.5, 1997. San Diego, CA: ANATECH Corp.

5. *ABAQUS Users Manual*, Version 5.8, 1998. Providence, RI: Hibbitt, Karlsson & Sorensen, Inc.

6. Klamerus, E. L., et al. 2001. "NUPEC/NRC PCCV Structural Behavior Test Model-Instrumentation Plan," Plan, Gage Locations, and Final As-Built Drawings, issued 1/31/01. Albuquerque, New Mexico: Sandia National Laboratories.

7. Eckelmeyer, K. H., Van Den Aryle, J. A., Kilgo, A. C. and Lambert, L. D. 2001. "Metallurgical Analysis of PCCV Liner Tears," Sandia Internal Report - Draft, October 26, 2001, Albuquerque, New Mexico: Sandia National Laboratories.

8. Hessheimer, M. F., Klamerus, E. W., Rightley, G. S., Lambert, L. D. and Dameron, R. A. 2003. *Overpressurization Test of a 1:4-Scale Prestressed Concrete Containment Vessel Model*, NUREG/CR-6810, SAND2003-0840P, Sandia National Laboratories, Albuquerque, NM.

9. Clauss, D. B., et al. 1987. *Round-Robin Pretest Analyses of 1:6 Scale Reinforced Concrete Containment Model Subject to Static Interval Pressurization*, SAND87-0891, NUREG/CR-4913, Albuquerque, NM: Sandia National Laboratories.

NRC FORM 335 (2-89) NRCM 1102, 3201, 3202

U.S. NUCLEAR REGULATORY COMMISSION

BIBLIOGRAPHIC DATA SHEET

(See instructions on the reverse)

1. REPORT NUMBER (Assigned by NRC, Add Vol., Supp.. Rev., and Addendum Numbers, if any)
NUREG/CR-6809
SAND2003-0839P
ANA-01-0330

2. TITLE AND SUBTITLE

Posttest Analyis of the NUPEC/NRC 1:4 Scale Prestressed Concrete Containment Vessel Model

3. DATE REPORT PUBLISHED

MONTH	YEAR
March	2003

4. FIN OR GRANT NUMBER
JCN Y6131

5. AUTHOR(S)

R. A. Dameron, B. E. Hansen, D. R. Parker and Y. R. Rashid

6. TYPE OF REPORT
Technical

7. PERIOD COVERED *(Inclusive Dates)*
Oct. 2000 to Sep. 2002

8. PERFORMING ORGANIZATION – NAME AND ADDRESS *(If NRC, provide Division, Office or Region, U.S. Nuclear Regulatory Commission, and mailing address; if contractor, provide name and mailing address.)*

Sandia National Laboratories, P.O. Box 5800, Albuquerque, NM, 87185-0744

9. SPONSORING ORGANIZATION – NAME AND ADDRESS *(If NRC, type "Same as above", if contractor, provide NRC Division, Office or Region, U.S. Nuclear Regulatory Commission, and mailing address.)*

Division of Engineering Technology
Office of Nuclear Regulatory Research
U. S. Nuclear Regulatory Commission
Washington, DC 20555-0001

10. SUPPLEMENTARY NOTES

11. ABSTRACT *(200 words or less)*

The Nuclear Power Engineering Corporation (NUPEC) of Japan and the U.S. Nuclear Regulatory Commission (NRC), Office of Nuclear Regulatory Research, co-sponsored a Cooperative Containment Research Program. Overpressure tests of a prestressed concrete containment vessel (PCCV) model began in July 2000, culminating in a functional failure mode or Limit State Test (LST) in September 2000 and a Structural Failure Mode Test (SFMT) in November 2001. The PCCV model, uniformly scaled at 1:4, is representative of the containment structure of an actual Pressurized Water Reactor (PWR) plan (OHI-3) in Japan. The objectives of the internal pressurization tests were to obtain measurement data of the structural response of the model to pressure loading beyond design basis accident in order to validate analytical modeling, to find pressure capacity of the model, and to observe its failure mechanisms.

This report compares results of pretest analytical studies of the PCCV model to the PCCV high pressure test measurements and describes results of post-test analytical studies. In addition to summarizing comparisons between measured behavior and predicted behavior of the liner, concrete, rebar, and tendons, a variety of failure modes and locations have been investigated.

12. KEY WORDS/DESCRIPTORS *(List words or phrases that will assist researchers in locating the report.)*

Containment
Severe Accidents
Pressure Testing
Finite Element Analysis

13. AVAILABILITY STATEMENT
unlimited

14. SECURITY CLASSIFICATION
(This Page)
Unclassified
(This Report)
Unclassified

15. NUMBER OF PAGES

16. PRICE

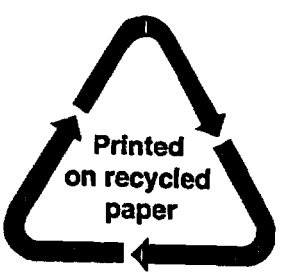

Federal Recycling Program

UNITED STATES
NUCLEAR REGULATORY COMMISSION
WASHINGTON, DC 20555-0001

OFFICIAL BUSINESS